DEVELOPMENT OF A POLARIMETRIC SPACE-TIME RADAR FOR AIRBORNE WEATHER HAZARD MONITORING

Yan Zhang*
University of Oklahoma, Norman, OK 73072

1. INTRODUCTION

The challenges of aviation hazard monitoring have been studied widely and many technologies have been developed (Mahapatra (1999)). The attention of this work focuses on the on-board sensing capabilities rather than relying on remote weather information data-links. The on-board weather sensors, if operated properly, are able to provide high-resolution, higher-data rate, and close-to-in-situ measurements *inside* individual radar resolution volumes. Therefore, on-board sensing capabilities can have great values for both military and civilian missions.

Two types of aviation weather hazards are of interest: (a) The mixed hydrometeor particles, which are generally detected and analyzed through polarimetric radar signatures (Vivekanandan (1993)), and (b) Air-motion related hazards. Motivated by the request from limited on-board space and power, this work attempts to study the possibility of developing a processing scheme in order to monitor multiple types of hazards simultaneous with a unified, reconfigurable sensor platform.

It is well-known that the Space-Time Adaptive Processing (STAP) has been applied to airborne phased array radars (Guerci (2003)) for detecting hard target from clutters. Showman (2003) discussed the approach to incorporate polarimetric measurement into STAP to enhance Ground Moving Target Indication (GMTI) detection performance. In Novak (1989) and Novak (1992), the optimal polarimetric detector and the polarimetric matched filter (PMF) are introduced. Polarimetric radar information is also incorporated into the time-frequency analysis techniques and the improvement in Angle-of-Arrival (AOA) estimation accuracies are demonstrated (Zhang (2006)). The above works, on the other hand, mainly address either detecting target from stationary ground-clutter, or resolving multiple targets in space with polarimetric data as another degree of freedom.

It is believed here that polarimetry-enhanced STAP can be used with *distributed* weather targets with *internal motions*. Based on an unified space-time-polarimetry framework, different kinds of state-vector configuration results in different hazard monitoring filters, which can be used for multiple tasks such as detecting air-traffic in instrumental meteorological condition (IMC), measuring wind hazards, as well as separating hydrometeor hazards (such as rain and icing) using joint space-polarimetry knowledge.

*Corresponding author: Yan Zhang, School of Electrical and Computer Engineering, University of Oklahoma, Norman OK 73072, Email: rockee@ou.edu

2. THE CONCEPTUAL RADAR SYSTEM OPERATION

A polarimetric array radar sensor is being designed by the University of Oklahoma (OU), which has a simple top-level system concept as shown in Figure 1. The sensor transmits, receives and digitalizes the dual-polarized signals from multiple antenna channels. A 3-D data cube can be constructed with indexes of (a) antenna (b) polarization state (c) pulse number. Since the receive elements are omni-directional, the field impinging on the antennas are superposition of hazards from various spatial locations. The system will rely on digital array processing to 'scan' the 3-D space and generate a comprehensive 'hazard map'.

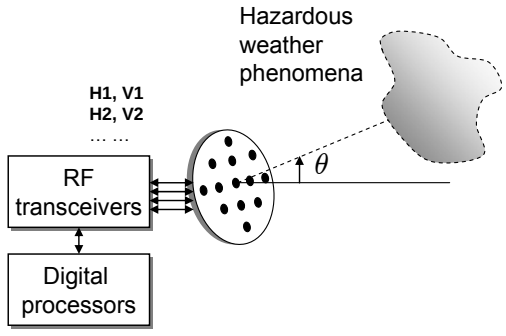

Figure 1 The conceptual operation for polarimetric space-time radar for aviation hazard monitoring

As one of the key technologies of such systems, the dual-polarized array antennas have already been used in some airborne radar applications (Skora (2005)). In our design, the digital beam-forming technique is suggested to avoid the complicated dual-polarized feeding network in the analog beamforming scheme, and to support the space-time processing algorithms. Polarimetric measurement can be obtained on a pulse-to-pulse switching basis (Santalla (2002)).

3. THE SPACE-TIME PROCESSING

3.1 Air-traffic Detection

For this case, assuming a radar resolution volume containing both win-driven distributed hydrometeors and air-traffic-type target, is observed by N receive antenna

channels with the same polarization and M pulses from each channel, we construct a MN×1 space-time vector $\mathbf{Z_n}$, and also construct MN×1 space time steering vector **st**, which predicts the phase distribution at each antenna element and each received pulse, using the notations of Guerci (2003), we have $\mathbf{st} = \mathbf{b} \otimes \mathbf{a}$, where **b** is the Doppler steering vector and **a** is the spatial steering vector. ⊗ denotes the Kronecker product.

The key to apply space-time processing to distributed target is the space-time covariance matrix defined as

$$\mathbf{Q} = E\{\mathbf{Z_n}\mathbf{Z_n^*}\} \quad (1)$$

, where E {·} represents statistical average and $\mathbf{Q}$ can be estimated through multiple-sections of training data samples. A simulation study is performed to investigate the structure of $\mathbf{Q}$ for an assumed airborne rain-fall target associated with different wind-fields. The rain-fall consists of numerous (>10^4) samples of spherical water drop scatterers with various sizes, and the total receive field is the combination of contributions from all the scatterers in the volume. It is observed that for the weather targets, the structure of $\mathbf{Q}$ matrix depends on the array configuration and observation geometries.

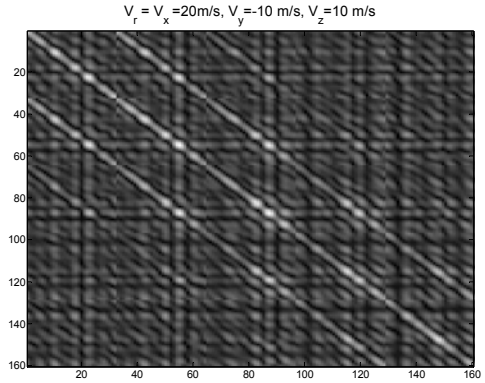

(a) $\|\mathbf{Q}\|$ when v_r is 20 m/s

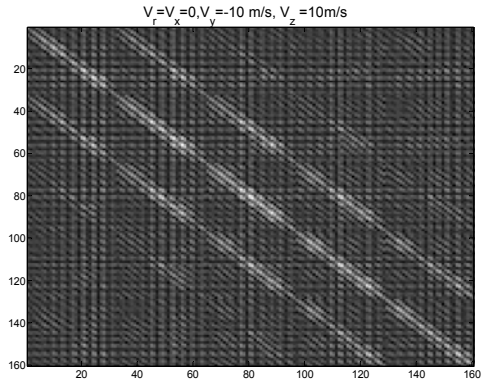

(b) $\|\mathbf{Q}\|$ when v_r is zero

Figure 2 The 2-D plot of $\|\mathbf{Q}\|$ for two different wind conditions (v_x as radial velocity) , v_y = -10 m/s and v_z = 10 m/s. All wind components have standard deviation (turbulence) $\sigma_{x,y,z}$ = 5 m/s. M=32, N=5 ($\lambda/2$ spacing).

For M=24 and N=5, an example is shown in Figure 2 to depict the impact of wind component on $\mathbf{Q}$. We can see that $\|\mathbf{Q}\|$ has N significant 'ridges', and as the ratio of tangential-wind to radial-wind increases, the ridges of $\|\mathbf{Q}\|$ becomes wider and the entire $\|\mathbf{Q}\|$ magnitude becomes smoother. A more useful tool to describe the impact of wind hazards is the eigenspectra, which is an orderly arrangement of eigenvalues of $\mathbf{Q}$**.** Simulation results show that turbulence and tangential wind widens the eigenspectra (in Figure 3).

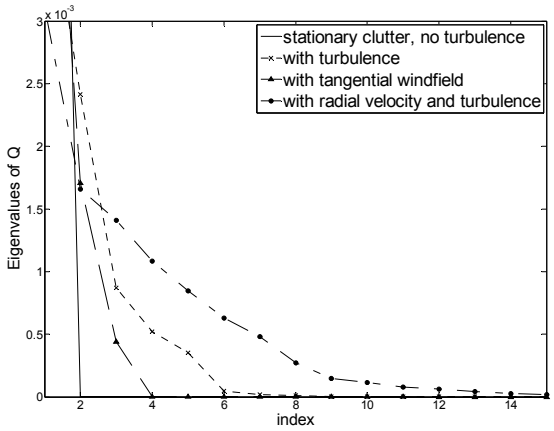

Figure 3 It is observed that stronger tangential wind fields and turbulence result in 'wider' space-time eigen-spectra. M = 24 and N = 3, the first 15 eigen-values are plotted.

Based on the above knowledge, the adaptive space-time processor should recursively estimate the $\mathbf{Q}$ from training observation cells and apply the optimal filtering (maximizing signal-to-clutter-ratio) to the volumes under surveillance:

$$y = \mathbf{z}_n^* \mathbf{w}_{opt} \quad (2)$$

, where $\mathbf{w}_{opt} = \kappa \mathbf{Q}^{-1}\mathbf{s}$, $\mathbf{s}$ is the desired signal vector, κ is a constant scalar.

For actual scenarios of detecting non-cooperative air-traffic in IMC condition, the location and velocities of the 'desired signal' is unknown, thus a *space-time scanning* approach is used as the basis of a practical algorithm. The procedure of this algorithm can be summarized as (1) estimating the wind vectors and the space-time covariance matrix $\mathbf{Q}$ for weather clutter, (2) construct the space-time steering vector $\mathbf{st}$ for each possible radial velocity v_r and θ (AOA), (3) for each v_r and AOA, compute the *space-time-spectrum*, under certain assumptions, the space-time-spectrum can be derived as

$$\begin{aligned} &\mathbf{P}(\theta, v_r) \\ &= E\left\{\left\|\mathbf{w'}_{opt}\mathbf{Z}_n\right\|^2\right\} \\ &= \mathbf{Z}_n \mathbf{st}(\theta, v_r) \cdot \mathbf{Q}^{-1} \cdot \mathbf{st}(\theta, v_r)^* \mathbf{Z_n^*} \end{aligned} \quad (3)$$

To illustrate the operation of the algorithm based on space-time-spectrum, a simulation example is run with an X-band radar resolution volume at 0° AOA containing rainfall scatterers. The wind-field velocities have Gaussian distribution with mean vector (20, 20, 30) m/s and standard deviation (10 10 10) m/s (turbulence). Assuming another 'specie' of scatterers (e.g., air-crafts, birds, etc.) locating inside the same cell at -10° azimuth direction and have mean velocity (-45, 20, 0) m/s and (10,10,0) m/s standard deviation, and the $\mathbf{Q}$ for weather targets is already known.

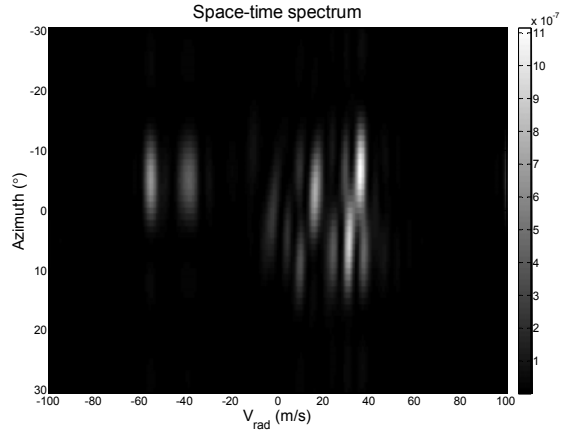

(a) $\mathbf{P}$ in (3) without $\mathbf{Q}^{-1}$ applied

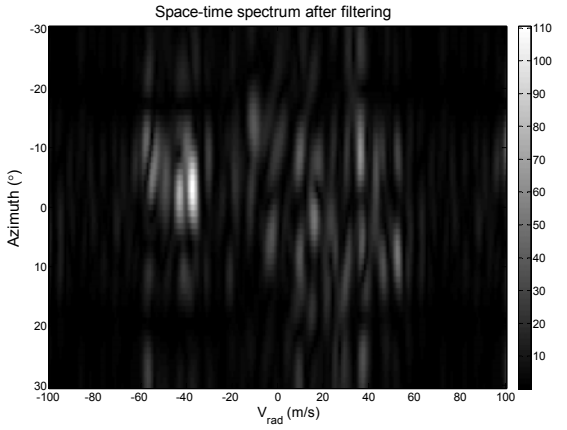

(b) $\mathbf{P}$ in (3) with $\mathbf{Q}^{-1}$ applied

Figure 4 Illustration of space-time filtering results on $\mathbf{P}$, for a simulated mixed hazardous scenario.

As we can see from Figure 4(a), before the space-time filtering, the weather clutter signature is 'spread' within certain velocity and angular regions. The reflectivity of the desired targets is relative weaker and overwhelmed. Applying the $\mathbf{Q}^{-1}$, on the other hand, suppresses the weather clutter and makes the desired target signature rise up as the highest peak in the 'spectrum map', the AOA of the desired target can be estimated simultaneously with its radial velocity.

The algorithm based on equation (3) assumes that the desired target signal and weather clutter are statistically uncorrelated to each other, also the weather field parameters during the observation time period remains constant. Thus the performance of space-time filtering on the distributed targets can be estimated relatively easier, as for given $\mathbf{Q}$, Klemm (2002) gives the boundaries of the optimal signal-to-clutter improvement factor (IF_{opt}) as

$$\frac{1}{\lambda_{\max}} tr(\mathbf{Q}) \le IF_{opt} \le \frac{1}{\lambda_{\min}} tr(\mathbf{Q}) \tag{4}$$

, where $tr()$ denotes the trace of a matrix and λ_{min}, λ_{max} are the minimum and maximum eigenvalues of $\mathbf{Q}$, respectively.

3.2 Wind-hazard Estimation

Wind-hazards, such as windshear, turbulence and strong up/down drafts, are major threats to aircrafts during different flight stages. Remote-sensing of the wind hazards, such as the F-factor estimation (Mahapatra (1999)), requires real-time estimation of both vertical and horizontal wind vectors as well as their time-derivatives. In order to accurately estimate $\mathbf{Q}$ for optimal space-time filtering as defined in (2), wind estimation is also a critical step. In this work, we use a simple interferometry approach to incorporate the wind-estimation into the space-time processing architecture. The interferometer or the correlation receiver multiplies time-delayed signals from one receive antenna with the signals from the other antenna, and feeds the results through a low-pass filter. For stable wind-fields (when the turbulence and windshear are weak), it can be shown that the output from low-pass filtering is a non-stationary process with numerous frequency components. The strongest frequency component has a frequency value of

$$f_{CF} = \frac{2\tau \bar{v}_{\tan}^2}{\lambda R_0} \tag{5}$$

, where τ is the time-delay between the two receive channels, λ is the radar operating wavelength, R_0 is the range of the scattering volume, and $\bar{v}_{\tan}$ is the mean tangential wind velocity. The tangential wind speeds can then be estimated from (5), and combined with radial velocity estimation from Doppler spectrum of a single channel to obtain a 2-D wind picture.

A Monte-Carlo simulation for a single radar scattering volume is performed for a 9.5-GHz airborne radar with 3° beam-width. The range-gate from pulse-width is 150 m and the range of the scattering volume is 1 km. 200 point scatterer sampling points are randomly placed in the radar resolution volume for each Monte-Carlo iterations. The correlation is passed through a low-pass filter with 1KHz cutoff frequency, and then a Burg spectrum estimation is performed on the low-pass filter's outputs. The radar line-

of-sight is at z direction, and the motions of the point scatterers are driven by an assumed wind-field relative to the aircraft, with different levels of standard deviations (σ). 10-iterations of Monte-Carlo simulations are performed and the results are averaged.

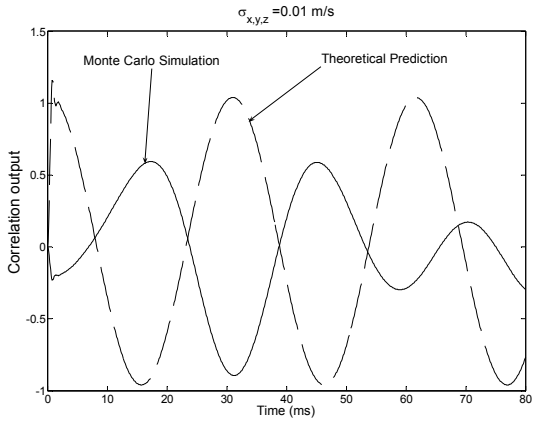

(a) Time-series waveform (I part) of correlation receiver output when σ = 0.01 m/s

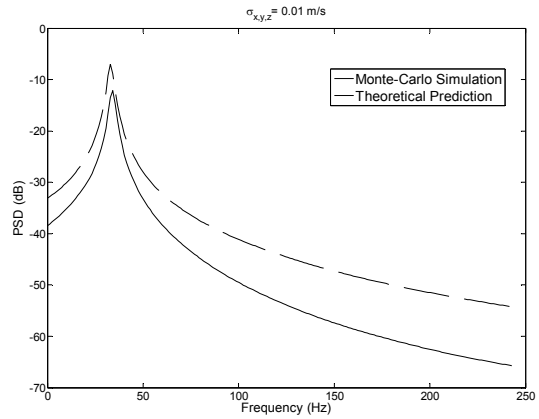

(b) Power spectrum density of correlation receiver output when σ = 0.01 m/s

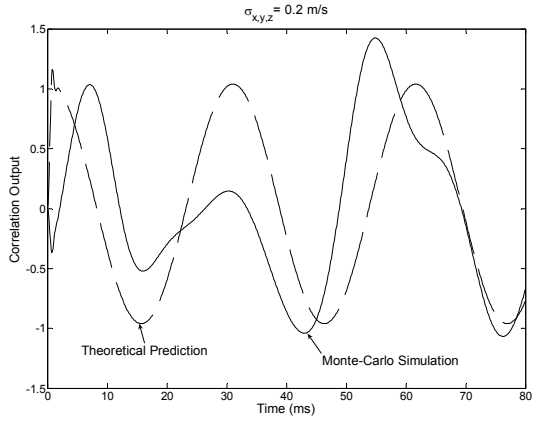

(c) Time-series waveform (I part) of correlation receiver output when σ = 0.2 m/s

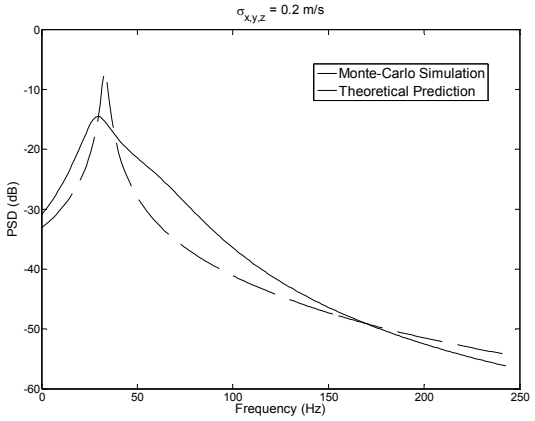

(d) Power spectrum density of correlation receiver output when σ = 0.2 m/s

Figure 5 Time-series waveforms and power spectrum density (PSD) of a simulated radar resolution volume with random scatterers and relative wind velocities v_x=v_y=70 m/s, v_z=150m/s. Radar operating frequency is 9.5 GHz.

Figure 5 shows the time-waveforms as well as the PSD of the low-pass filter output for σ=0.01 m/s and 0.2 m/s, respectively. It is observed that when the σ is small, the Monte-Carlo simulation results match the theoretical prediction very well, and the estimation error of $\bar{v}_{\tan}$ based on (5) is about 5 m/s. The increase in σ, however, gives rise to other frequency components and makes the PSD become 'flat'.

The characteristic frequency f_{CF} is such a low frequency that it does not have significant impact on the long-range, lower frequency radars. While for an airborne radar operating at shorter range to weather hazards, it is possible to extract f_{CF} as long as the observation time is sufficient. The Micro-Doppler processing introduced in Chen (2006) may be a good solution for this case.

4. THE SPACE-POLARIMETRY PROCESSING

Assuming mixed weather hazards (rain, snow or hail) locate at some unknown directions (θ), and we hope to detect the existence of one of them from others. Polarimetric information will be needed for this case. Suppose the antenna array consists of N elements and at a given time t_0, each channel i produces a zero-mean Gaussian polarimetric signal vector

$$\mathbf{X_i} = \left[\begin{array}{ccc} \mathrm{HH}_i & \mathrm{HV}_i & \mathrm{VV}_i \end{array} \right]' \qquad (6)$$

, and a space-polarimetry signal vector with length 3N can be constructed as

$$\mathbf{X_p} = \left[\begin{array}{cccc} \mathbf{X_1} & \mathbf{X_2} & \ldots & \mathbf{X_N} \end{array} \right]' \qquad (7)$$

The space-polarimetry covariance matrix can be defined as

$$\mathbf{Q}_p = E\left\{\mathbf{X}_p \mathbf{X}_p^*\right\} \tag{8}$$

, which can be shown to have a structure

$$\mathbf{Q}_p = \begin{bmatrix} \mathbf{R}_p(\theta) & \mathbf{R}_{12}(\theta) & \cdots & \mathbf{R}_{1N}(\theta) \\ \mathbf{R}_{21}(\theta) & \mathbf{R}_p(\theta) & \cdots & \mathbf{R}_{2N}(\theta) \\ \vdots & \vdots & \ddots & \vdots \\ \mathbf{R}_{N1}(\theta) & \mathbf{R}_{N2}(\theta) & \cdots & \mathbf{R}_p(\theta) \end{bmatrix} \tag{9}$$

, where (Novak(1992))

$$\mathbf{R}_p(\theta) = \sigma \begin{bmatrix} 1 & 0 & \rho\sqrt{\gamma} \\ 0 & \varepsilon & 0 \\ \rho^*\sqrt{\gamma} & 0 & \gamma \end{bmatrix} \tag{10}$$

, and

$$\mathbf{R}_{ij}(\theta) = \begin{cases} \mathbf{R}_p(\theta) \cdot e^{j2\pi \frac{d \sin\theta}{\lambda}}, \mathrm{i} < \mathrm{j} \\ \mathbf{R}_p^*(\theta) \cdot e^{-j2\pi \frac{d \sin\theta}{\lambda}}, \mathrm{i} > \mathrm{j} \end{cases} \tag{11}$$

The four parameters σ (ZR), ε (LDR), γ(ZDR) and ρ (ρ_{hv}) are the feature parameters for target/clutter characterization. It is emphasized here that these four parameters are functions of θ for meteorological targets, and multiple-types of hazards from different AOAs may belong to different species. Therefore, joint-space-polarimetry processing is useful to generate the 'merged' hazard information which is not available for space-only or polarimetry-only processing.

A *meteorological scatterer knowledge-base* (MSKB) can be established and used to predict the AOA-dependence of the polarimetric parameters. Figure 5 shows the basic geometry for a simulated hail-type scattering case. The complex radar cross section (Riegger (1989)) of a single scatterer is calculated using the finite element method (FEM). Figure 6 depicts the results of the HH scattering component for different particle sizes.

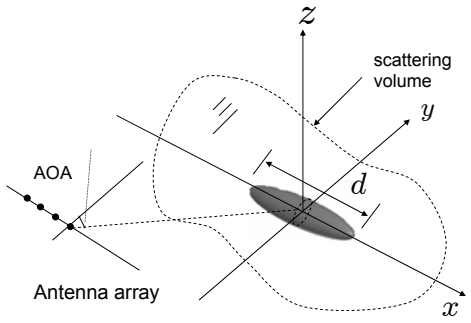

Figure 6 A simulated meteorological scattering case: a hail-type ice-spheroid with length *d* at main axis and 5:1 axis ratio. The scatterer is within a volume at a specific AOA relative to the antenna array.

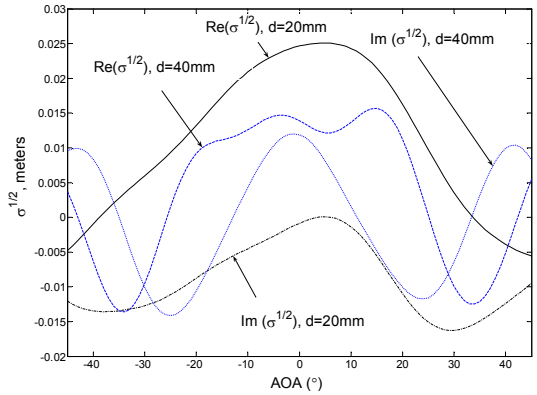

(a) Monostatic complex RCS of the spheroid with d=20 mm and 40 mm, respectively.

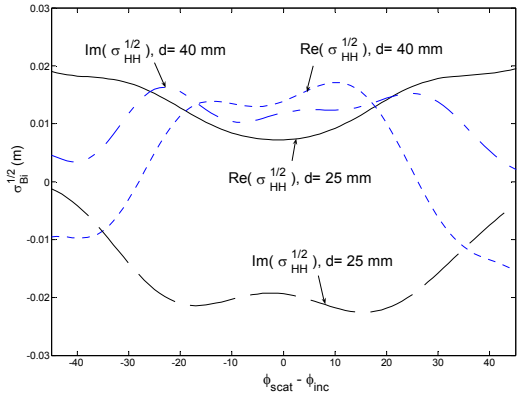

(a) Bi-static complex RCS of the spheroid with d=25 mm and 40 mm, respectively.

Figure 7 The dependence of $\sqrt{\sigma_{HH}}$ on AOA and scattering angle, of the simulated hailstone for both mono-static and bi-static cases.

The data in Figure 6(a) can be used in MKSB and assist the prediction of polarimetric parameters from different angles. Also from Figure 6(b), we can observe a slight variation of RCS at different receive array element, due to the small variations of the scattering angles from the target. However, this variation is so small that it can be either compensated or ignored.

Similar to the space-time processing, an optimal weighting $\mathbf{w_{opt}}$ can be applied to the signal vector $\mathbf{X_p}$ at given clutter covariance $\mathbf{Q_{pc}}$ and scanning variable θ, the space-polarimetry filtering will generate a 1-D notch-filtered spectrum as

$$\mathbf{P}_{pn}(\theta) = \mathbf{X}_p \mathbf{a}(\theta) \cdot \mathbf{Q}_{pc}^{-1} \mathbf{a}^*(\theta) \mathbf{X}_p^* \tag{12}$$

, or on the other hand, generate a matched-filtered spectrum, with the assumed hazard covariance $\mathbf{Q_{ps}}$:

$$\mathbf{P}_{pm}(\theta) = \mathbf{X}_p \mathbf{a}(\theta) \cdot \mathbf{Q}_{ps} \mathbf{a}^*(\theta) \mathbf{X}_p^* \tag{13}$$

$\mathbf{a}(\theta)$ is the spatial steering vector In equations (12) and (13).

5. Conclusions

A unified polarimetric array radar architecture provides true potential of multi-functional external hazard detection and monitoring by allowing simultaneous space-time and space-polarimetry processing. With the space-time processing, it is possible to characterize the wind-hazards and detect external air-traffics from heavy weather clutters. The space-polarimetry processing is used to discriminate different types of hydrometeors. More practical algorithms and hardware systems are being developed.

6. ACKNOWLEDGEMENT

This work is partially supported by NASA-Langley Research Center (grant # NNX07AN15A). The author appreciate greatly for the comments and guidance from Dr. Robert Neece, Mr. Steven Harrach and other NASA researchers. This work also received important help from the National Severe Storm Laboratory (NSSL) and the members of the Atmospheric Radar Research Center (ARRC), in the University of Oklahoma.

7. REFERENCES

Chen, V.C., Li, F., Ho, S.-S., Wechsler, H., 2006: Micro-Doppler effect in radar: phenomenon, model, and simulation study, IEEE Trans. on Aerospace and Electronic Systems, 42(1), 2-21.

Guerci, J.R., 2003: Space-Time Adaptive processing, Artech House, Inc.

Klemm, R., 2002: Principles of Space-Time Adaptive Processing, The Institution of Electrical Engineers.

Mahapatra, P., 1999: Aviation Weather Surveillance Systems, The Institution of Electrical Engineers.

Novak, L.M., Sechtin, M.B., Cardullo, M.J., 1989: Studies of Target Detection Algorithms That Use Polarimetric Radar Data, IEEE Trans. on Aerospace and Electronic Systems, 25(2), 150-165.

Novak, L.M., Burl, M.C., and Irving, W.W., 1992: Optimal Polarimetric Processing for Enhanced Target Detection, IEEE Trans. on Aerospace and Electronic Systems, 29(1), 234-244.

Santalla, V., and Antar,Y.M., 2002: A Comparison Between Different Polarimetric Measurement Schemes, IEEE Trans, on Geoscience and Remote Sensing, 40(5), 1007-1017.

Showman, G.A., Melvin, W.L., and Belenkii, M., 2003: Performance Evaluation of Two Polarimetric STAP Architectures, Proceedings of the 2003 IEEE Radar Conference, 59-65.

Skora J., Sanz, A., and Fabbra, R., 2005: Dual polarized phased array antenna for airborne L-band SAR, Proceedings of IEEE MTT-S Int. Con., 192-196.

Vivekanandan, J., and Raghavan, R., 1993: Polarimetric Radar Modeling of Mixtures of Precipitation Particles, IEEE Trans. on Geoscience and Remote Sensing, 31(5), 1017-1030.

Zhang, Y., Obeidat, B.A., and Amin, M.G., 2006: Spatial Polarimetric Time-Frequency Distributions for Direction-of-Arrival Estimations, IEEE Trans. on Signal Processing, 54(4), 1327-1340.

Riegger, S. and Wiesbeck, W., 1989: Wide-band Polarimetry and Complex Radar Cross Section Signatures, Proceedings of the IEEE, 77(5), 649-658.